Improvement of wear and corrosion protection of PEO on AA2024 via sol-gel sealing

Luciane Sopchenski [a,b,*], Julien Robert [c], Matthieu Touzin [d], Arnaud Tricoteaux [c], Marie-Georges Olivier [a]

[a] Department of Materials Science, Faculty of Engineering, University of Mons, Place du Parc 20, 7000 Mons, Belgium
[b] Department of Metallurgy, Faculty of Engineering, University of Mons, 7000 Mons, Belgium
[c] LMCPA, Université Polytechnique Hauts de France, Bd Charles de Gaulle, 59600 Maubeuge, France
[d] Univ. Lille, CNRS, INRAE, Centrale Lille, UMR 8207 - UMET - Unité Matériaux et Transformations, F-59000 Lille, France

ABSTRACT

Plasma electrolytic oxidation (PEO) is a versatile and cost-effective technique to obtain protective oxide coatings in light metals, although its intrinsic porosity is a drawback for long-term corrosion resistance. Sol-gel layers are pointed as a useful tool to seal PEO porosity and increase its corrosion resistance, although little is known about its influence on the wear performance of PEO coatings. In this study, a PEO coating obtained on AA2024 was sealed with a hybrid sol-gel via dip-coating. Two withdrawal speeds were set in order to investigate the influence of the sol-gel filling in its sealing ability. Both sol-gel application conditions were able to fill the PEO pores and microcracks and change its wettability. EIS results showed samples sealed with sol-gel maintained the protective behavior upon 28 days and increased the resistance of the system by several orders of magnitude in comparison to unsealed PEO coatings. Pin-on-disk tests indicate the sol-gel decrease the shear stresses of the coating, decreasing its wear rate in 40% compared to the unsealed PEO.

1. Introduction

Aluminum alloys are extensively used in aerospace, especially the series 2xxx (with Cu as the main alloying compound). These alloys offer improved mechanical properties compared to bare aluminum (AA1050) but reduce their localized corrosion resistance [1,2]. Despite their improved mechanical properties, AA2024 possesses low wear resistance, requiring surface treatments to ensure its adequate performance [3].

Plasma electrolytic oxidation (PEO) is an environmentally friendly, versatile, and cost-effective electrochemical technique to obtain protective oxide layers in lightweight metals and alloys [4,5]. PEO coatings are formed under a complex mechanism that combines electrochemical reactions, plasma reactions, and thermal diffusion [6]. During the oxidation, numerous short-lived micro-discharges take place over the metal surface. The PEO micro-discharges abruptly increase in the local temperature and pressure and provoke the oxide to melt and solidify repeatedly, promoting the incorporation of species from the electrolyte and allowing the formation of high-temperature oxide phases [7,8]. The oxide coating produced by PEO is usually crystalline, has good adhesion to the substrate, and high hardness, resulting in a coating that improves wear resistance against fretting, abrasion, and erosion in aluminum alloys [9–12].

In the case of the AA2024 alloy, several works have been devoted to understanding the growth mechanism of the PEO layer, with particular attention given to the investigation of the influence of the electrical sign [13–17] and electrolyte composition [18–20] on the structural properties of the coating. Electrolytes composed of alkaline solutions with the addition of silicates, phosphates, or aluminates are commonly used [21–23]. Diluted KOH (or NaOH) increases the electrolyte conductivity, and the additives allow the micro-discharges to be formed at lower potentials. Components from the electrolyte, such as SiO_3^{2-}, PO_4^{3-}, and AlO_2^- increase the coating growth rate and can be incorporated on the coating composition [24].

Similar to PEO coatings in other aluminum alloys, PEO coatings on AA2024 improve the surface's tribological properties, reduce the weight loss after wear test, and decrease the friction coefficient and wear rate [25–27]. Xue et al. showed AA2024 PEO coatings reduced in three

orders of magnitude the wear rate in comparison to the bare substrate. The authors also showed the friction coefficient varies according to the coating's depth, depending on the crystalline structure and the layer's porosity [28].

When in contact with an aggressive medium, the PEO porosity is a drawback to the coating's corrosion resistance. PEO coatings on AA2024 grant limited corrosion resistance after short periods of contact with corrosive species. Fattah-alhosseini et al. showed AA2024 PEO coatings obtained with small amounts of sodium phosphate presented a corrosion resistance 48 times higher than the uncoated substrate after 2 h of immersion in 3.5 wt% NaCl [18]. After extended exposure to an aggressive medium, the electrolyte can penetrate through the PEO micro-cracks and porosity and initiate the corrosion process on the interface coating/substrate. Wen et al. investigated the corrosion process of an AA2024 PEO coating and observed a modulus of the impedance at low frequency 10 times higher in coated samples in comparison to the bare substrate on the first 6 h of immersion in 3.5 wt% NaCl [29]. However, after 24 h of immersion EIS results show the start of localized corrosion due to the electrolyte penetration on the cracks, pores, and coating defects. After immersion for 96 h, corrosion products were observed. The degradation of the corrosion resistance of AA2024 PEO coatings, after extended periods in contact with aggressive media was also observed by Del Olmo et al. [22]. The authors showed the possibility of incorporating corrosion inhibitors during flash-PEO and observed an increase of the corrosion resistance at short immersion periods. Although, after 28 days of immersion, the corrosion resistance of the PEO with and without corrosion inhibitors decreased due to the penetration of the electrolyte into the pores and the degradation of the outer porous layer.

Different post-treatments are employed to seal PEO's micro-cracks and pores to avoid the penetration of aggressive species and increase its corrosion resistance [16,30,31]. Hydrothermal treatments and rare-earth conversion coatings seal the PEO pores by the precipitation of products with low solubility [32–34]. Although, the precipitated products are prone to detachment and redissolution over time, impairing permanent corrosion protection.

Sol-gel coatings are pointed as a versatile sealing layer for PEO coatings considering the ease of fabrication, low environmental impact, and flexibility of the process. During the application, the sol-gel solution can penetrate into the cracks and pores of the PEO coating and provide a homogeneous protective layer over the entire PEO surface. The sealing performance of sol-gel layers on PEO coatings is well described, especially for magnesium and titanium alloys [35,36]. Farshid and Kharaziha reviewed the use of PEO/sol-gel coatings over different magnesium alloys and showed sol-gel based on different precursors (such as TiO_2, SiO_2, ZrO_2) were able to improve the corrosion resistance of distinct PEO coatings by filling their pores and micro-cracks [37]. Toorani and Aliofkhazraei summarized the results of sol-gel applied by different methods on magnesium PEO coatings and showed controversial findings related to the optimal sol-gel thickness for corrosion protection [36]. The authors stated multilayers, and thick sol-gel coatings tend to present microcracks due to thermal stress during the curing step; therefore, thin sol-gel layers are expected to have better sealing abilities. Contrarily, Duan et al. suggest applying multiple sol-gel layers could avoid structural defects caused by inadequate solvent evaporation and inadequate filling of the PEO pores [38]. Additionally, the sol-gel application under low pressure could avoid defects caused by residual air trapped in the PEO pores. Shang et al. showed the use of high humidity gelation conditions and the presence of ZrO_2 on the sol-gel composition reduces the presence of cracks caused by the thermal stress during the curing step [39].

Despite the extensive description of the use of sol-gel as a sealant layers for PEO coatings, scarce studies are found for its application on aluminum alloys. Pezzato et al. showed silica sol-gel layers decrease the wettability and increase the corrosion resistance of PEO coatings obtained on AA7020 alloys [40]. Zeng et al. showed the protective nature of sol-gel layer over an Al-Zn-Mg-Cu alloy, although no description of

the stability of those layers over time was provided [41]. Bouali et al. used an alumina-based xerogel layer as an intermediate treatment to the growth of LDH layers on AA2024, the authors showed the xerogel layer was able to improve the corrosion resistance of the PEO coating for short periods, although the protection was lost after 168 h of immersion in 0.5% NaCl [42]. To the best of found knowledge there is no report of the use of sol-gel layers to increase the barrier resistance of AA2024 PEO coatings on the literature.

In this paper, the sealing ability of a sol-gel layer over a PEO on AA2024 is presented. The sol-gel was applied via dip-coating using two withdrawal rates to obtain different sol-gel quantities entrained on the PEO coating. The influence of the sol-gel filling on the long-term protective behavior was investigated. The effect of sol-gel sealing on the tribological properties of the coating was also assessed.

2. Experimental procedures

AA2024 alloy with the nominal composition of 3.8–4.9% Cu, 1.2–1.8% Mg, 0.3–0.9% Mn, ≤0.5% Fe, ≤0.5% Si, ≤0.25% Zn, ≤0.15% Ni, ≤0.15% Ti, and Al balance, was used as the substrate in the present study. Before the PEO, AA2024 specimens (30 mm × 30 mm × 1.6 mm) were ultrasonically cleaned in acetone for 10 min. The samples were then etched in alkaline solution (NaOH at 40 °C for 30 s) followed by a bath in an acid dismutting solution (HNO_3 at room temperature for 30 s).

The PEO process was carried out by utilizing a bipolar power supply (PowerPulse - Micronics, France) using a squared pulsed regime with 5 A of anodic current, 30% duty cycle and 100 Hz for 30 min. The oxidation was performed in a 3 litres double jacketed cell connected to a cryostat. The electrolyte temperature was controlled to be below 40 °C. A stainless-steel plate (360 cm^2) was used as a counter electrode, and an aqueous solution containing 1 g/L KOH and 1.65 g/L Na_2SiO_3 was used as the electrolyte.

The sol-gel composition was selected by its performance on sealing anodized aluminum alloys [43]. Briefly, the sol-gel was composed by 10% v/v of 3-glycidyloxypropyl-trimethoxysilane (GPTMS, Alfa Aesar) and 20% v/v of tetraethoxysilane (TEOS, VWR), in a solution of ethanol and distilled water. For the acid-catalysis process acetic acid was used to adjust the pH to 2.3–2.5. After 2 h of hydrolysis under agitation, the sol gel was applied via dip-coating and cured at 150 °C for 1 h. In order to evaluate the influence of the sol-gel sealing ability over the PEO coatings, the application was performed using two different withdraw speeds, 100 and 200 mm/min. Samples were named PEO, PEO SG 100 (sol-gel applied at 100 mm/min), and PEO SG 200 (sol-gel applied at 200 mm/min).

The coating's morphology and chemical composition were analyzed by scanning electron microscopy (SEM) equipped with an energy dispersive X-ray spectroscopy (EDX) module (Hitachi SU8020 - Hitachi, Japan and JEOL JSM-7800F LV, Japan). Sample cross-sections were observed by SEM on samples mounted in resin and abraded (#800, #1200 SiC paper) and polished with diamond paste (1 μm). The crystalline structure of the PEO coatings was analyzed by grazing incidence X-ray diffraction (GIXRD) with an incident angle of 0.5°, a step size of 0.05°, and a counting time of 11 s (Panalytical Empyrean - Malvern Panalytical, UK). The coatings wettability was assessed by sessile-drop goniometry using 1 μL of deionized water in a contact angle goniometer. Five measurements were done for each group of samples.

Wear resistance of the PEO coatings was evaluated by using a pin on disk tribometer (TRIBOtechnics, France) under dry conditions at room temperature. A 6 mm alumina ball was used as counterbody. The normal load, the track radius, the sliding speed and the sliding distance were equal to 1 N, 3 mm, 50 mm.s^{-1} and 4000 m, respectively. Before testing, the counterbody was cleaned with alcohol and the contact surface of the alumina ball was renewed. The tangential forces were measured to calculate the friction coefficients. Three tests were carried out for each specimen. The first two tests were stopped at 750 m and the third one
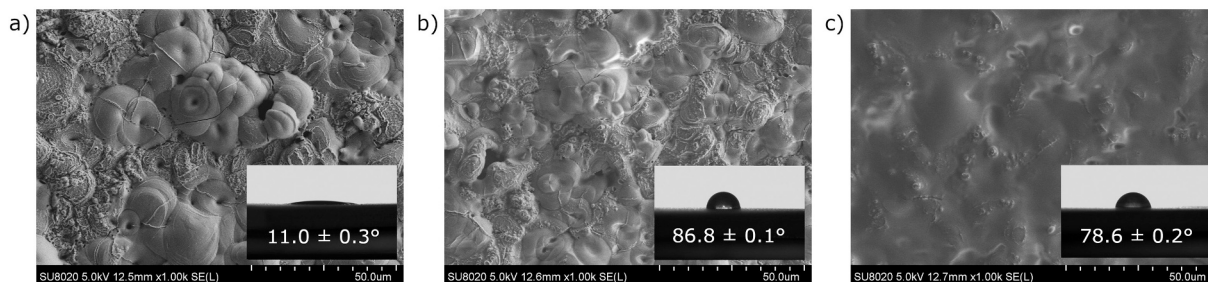
Fig. 1. Top-view SEM images of the unsealed PEO coating (a), PEO coating sealed with sol-gel applied at 100 mm/min (b) and 200 mm/min (c). The insert shows the contact angle measurements.

Table 1
Chemical composition of the coatings assessed by EDX.

Sample	Composition (% at.)						
	Al	O	Mg	Cu	Si	Na	K
PEO	32.0 ± 0.4	61.0 ± 0.9	0.5 ± 0.1	0.5 ± 0.2	3.6 ± 0.1	0.5 ± 0.1	0.5 ± 0.1
PEO SG 100	28.9 ± 0.3	59.9 ± 0.9	0.5 ± 0.1	0.4 ± 0.2	4.9 ± 0.2	0.2 ± 0.1	0.3 ± 0.1
PEO SG 200	16.7 ± 0.3	54.3 ± 0.9	0.4 ± 0.1	0.2 ± 0.2	12.7 ± 0.2	0.3 ± 0.1	0.3 ± 0.1

was ended at 4000 m to measure the wear volume, since 750 m sliding distance was not long enough to quantify accurately the wear volumes.

3D topographic analysis of the surfaces of the specimens before wear tests and of the wear tracks profiles were carried out by confocal microscopy with a LEICA DCM 3D confocal microscope (Germany). Surface roughness was measured according to ISO 4287 standard procedure. The wear volume loss was calculated from the profiles of the wear tracks. Eight profiles were analyzed on the three circular wear tracks for each specimen. The average hollow value extracted from the profiles was multiplied by the circumference of the wear tracks to calculate the wear loss.

The specific wear rate was then calculated according to the following relation (Eq. (1)):

$$K = \frac{V}{F.s} \tag{1}$$

where V is the volume loss in mm^3, F the normal load in N and s the total sliding distance in m.

The corrosion protection performance of the coatings was assessed by electrochemical impedance spectroscopy (EIS) using a three-electrode cell inside of a faraday cage. The samples were placed as the working electrode along with an Ag/AgCl/KCl (+197 mV/SHE) reference electrode and a platinum counter electrode. A rounded area of 1 cm^2 of the working electrode was exposed to the electrolytic solution (0.1 M Na$_2$SO$_4$). This electrolyte was chosen to limit the corrosion attack at the aluminum interface and to highlight the barrier properties of the duplex coating. Before the EIS measurement the open circuit potential was recorded for 30 min. The EIS was performed using a BioLogic SP-300, from 10^5 Hz to 10^{-1} Hz, with 10 mV of amplitude signal voltage, and 10 points recorded per decade. The experimental data were fitted to electrical equivalent circuits (EEC) using ZView electrochemical
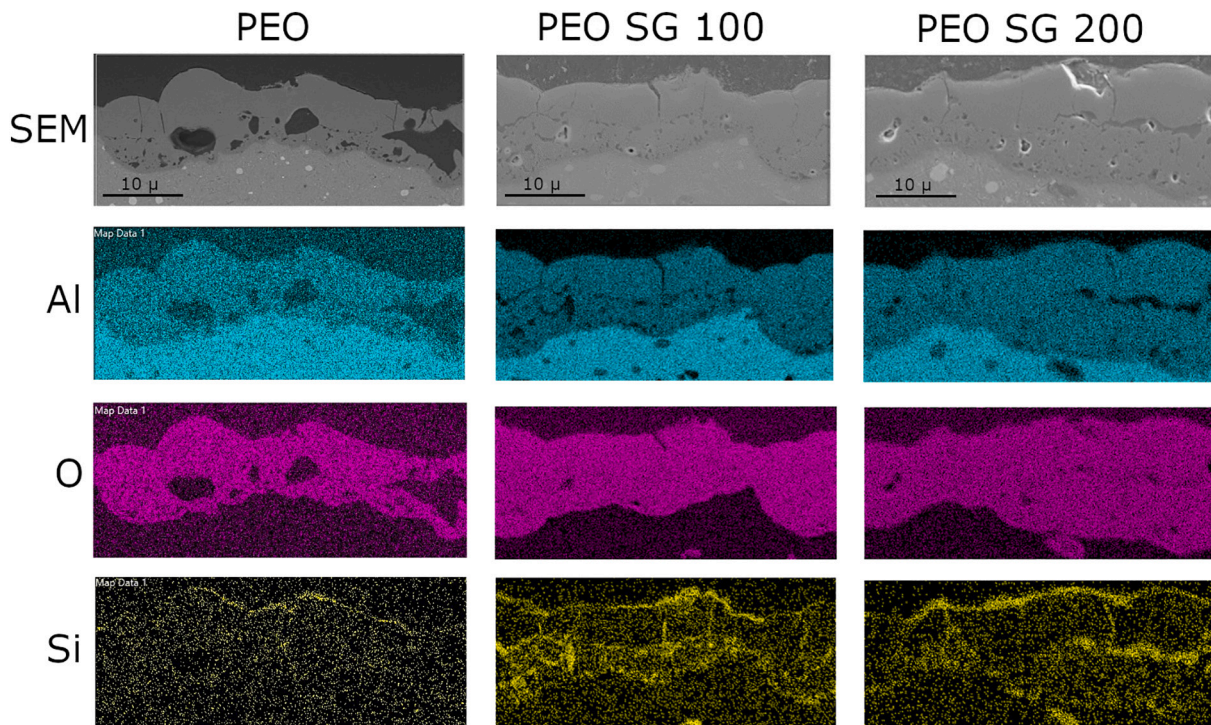

Fig. 2. Cross-section SEM images and EDX mapping of PEO coating, and PEO coatings sealed with sol-gel applied at 100 mm/min (PEO SG 100) and 200 mm/min (PEO SG 200).
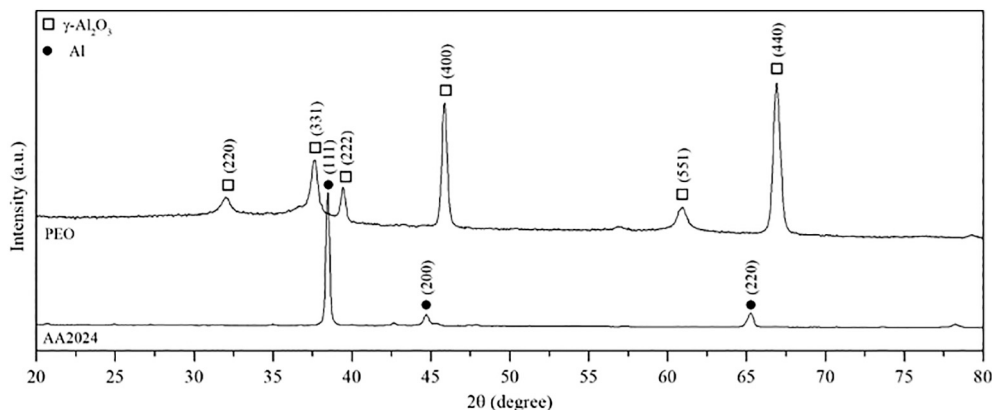
Fig. 3. XRD patterns of the substrate (AA2024) and the PEO coating.

Table 2
Sol-gel thickness and 3D topographic results.

Sample	Sz (µm)	Sku	Sol-gel thickness (nm)
PEO	71.0	29.4	–
PEO SG 100	41.6	6.9	438 ± 21
PEO SG 200	44.6	9.4	696 ± 192

analysis software. In order to check results reproducibility, at least two measurements were done for each sample group.

3. Results

SEM top-view images of the coatings are shown in Fig. 1. The PEO coating surface presents features typical from aluminum alloys oxidized in silicate-containing electrolytes, Fig. 1a [44–46]. Innumerous pores ranging from 1 to 10 µm of diameter, randomly distributed on the surface, are present due to the formation of plasma channels during the PEO process. It is also possible to observe microcracks radially oriented in respect to the pores, originated from thermal stress due to the continuous melting/solidifying process during the coating growth [46]. The sol-gel applied at 100 mm/min covered the PEO features, although it is still possible to observe some large pores and microcracks, Fig. 1b. The pores and features become less evident on the samples that received the sol-gel applied at 200 mm/min, Fig. 1c. The sol-gel coating decreased the surface's wettability as shown in the inserts of Fig. 1. The sol-gel

Fig. 4. Friction Coefficient for PEO specimens and substrate against sliding distance.

deposition increased the contact angle from 11° to 86 and 78° for the sol-gel applied at 100 and 200 mm/min, respectively. The increased hydrophobicity of the sample that received the sol-gel applied at 100 mm/min indicates despite the porosity is still visible, the sol-gel was able to penetrate the pores. Similar results were described by Pezzato et al., that observed an increase in the contact angle for uniform sol-gel layers applied in highly porous PEO coatings on magnesium alloys [40].

Simultaneously to the acquisition of SEM top-view images, the EDX elemental composition spectra were collected, Table 1. It can be noted the presence of elements from the substrate (Al, Mg and Cu), as well as elements from the electrolyte (Si, Na and K) that were incorporated in the coating during the oxidation. In good agreement with the SEM images, PEO samples sealed with sol-gel presented a higher amount of Si and a smaller amount of Al, due to the change in the interaction depth of EDX.

Fig. 2 presents the cross-section images of the samples along with the EDX mapping results. The PEO coating varies in thickness (18.9 ± 9.0 µm) and contains an interconnected network of pores that include voids between the external and internal layers, in good agreement with the literature [47,48]. The EDX map of the PEO layer shows the presence of a silicon-rich layer on the surface of the coating, characteristic of PEO coatings obtained in dilute alkaline-silicate electrolytes [49]. The EDX mapping of the PEO coatings sealed with sol-gel shows a higher presence of silicon and oxygen inside the pores, indicating the sol-gel covered the surface and infiltrated into the pores network, internally filling the pores and the microcracks.

The grazing incidence XRD patterns of the AA2024 substrate and PEO coating are shown in Fig. 3. PEO coatings obtained on aluminum alloys are usually mainly composed of α-Al_2O_3 and γ-Al_2O_3, although some researchers have described amorphous alumina PEO layers [28,50]. During the first stages of PEO, the oxide growing mechanism is analogous to the anodic oxidation. When the micro arcing starts to occur, the temperature increases abruptly due to the formation of plasma channels, reaching 10,000 K [51]. The high temperature allows the initial oxide layer to be transformed into the metastable γ-Al_2O_3 phase. Extended oxidation periods or higher current densities, allowing the transformation of γ-Al_2O_3 into α-Al_2O_3 [52,53]. The PEO XRD pattern in Fig. 3 shows the sole presence of peaks ascribed to the phase γ-Al_2O_3 [54]. Peaks from the aluminum cannot be observed since the grazing X-ray did not reach the substrate.

3D topographic analysis results and coating thicknesses are shown in Table 2. Sz parameter corresponds to the sum of the maximum peak height and the maximum valley depth. The Sku parameter also called *Kurtosis* value is a measure of the sharpness of the roughness profile [55]. High value of Sku means sharper roughness profiles (Gaussian profile corresponds to Sku = 3). The results in Table 2 show high values of Sku indicating predominance of non-Gaussian distribution of high peaks and deep valleys. Moreover, the significant decrease of the Sz and
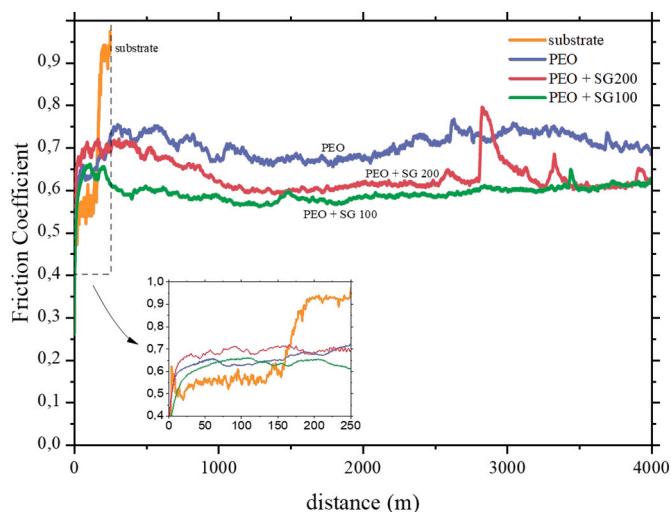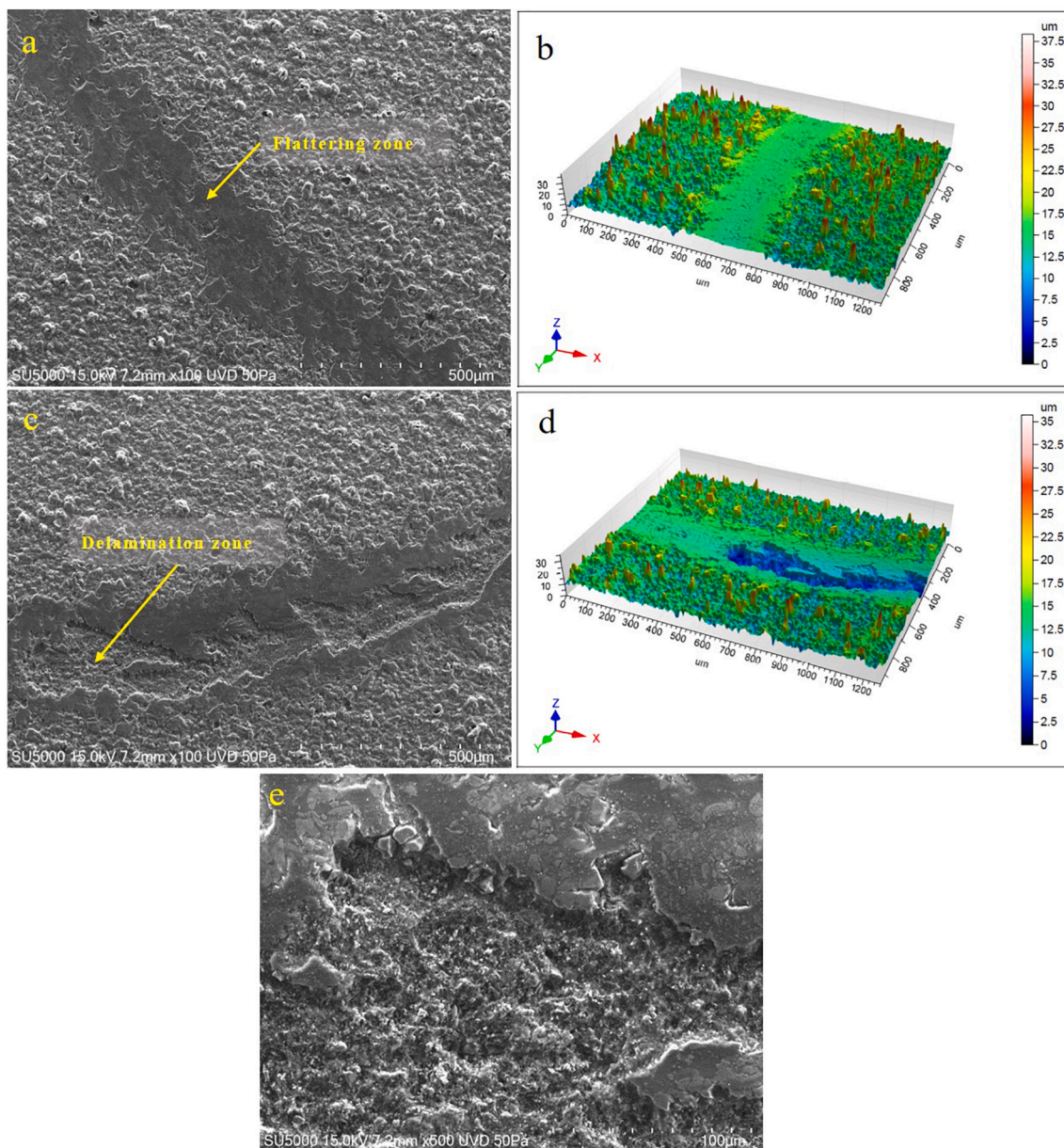
Fig. 5. Wear tracks obtained by SEM and wear 3D topographic surfaces obtained by confocal microscopy for PEO specimen. (a) and (b) flattering zone. (c) and (d) delamination zone. (e) magnification of the delamination zone.

Sku parameters in the case of PEO SG coatings is probably related to filling of the hollows with the sol-gel.

The sol-gel thickness was measured by cross-section SEM images along with EDX maps. During dip-coating, the withdrawal speed sets the sol-gel thickness, where higher speeds result in thicker coatings [56]. To this extent, the thicknesses of the sol-gel applied at 100 and 200 mm/min are in good agreement with the theory, although the sol-gel coating obtained at 200 mm/min presented a heterogeneous thickness as shown by the high standard deviation value.

Fig. 4 shows the variations of the friction coefficients as a function of the sliding distance for the PEO specimens and for the substrate during the longest tests (4000 m sliding distance). The variations of the friction coefficients for the shorter tests (750 m sliding distance) are not depicted in Fig. 4. but are similar. The friction coefficient against the bare substrate is lower than that of the PEO and PEO SG coatings at the beginning of the wear test but increases rapidly to 0.9. During this first period, stick-slip phenomena are observed corresponding to detachment of asperities and probably adhesion on alumina counterbody. During the

second period (when sliding distance exceeds 200 m), ploughing in the aluminum is highlighted resulting in a high friction coefficient. Nie et al. measured similar friction coefficients for steel and WC-Co against aluminum alloy when the wear mechanism is defined as ploughing [57]. It can be observed that the friction coefficients increase at the beginning of the tests and then decrease. Then the friction coefficients remain almost constant for PEO SG samples between 0.6 and 0.65 contrary to the PEO sample for which variations can be observed at upper level between 0.65 and 0.75 which is similar to the results obtained by Li et al. [58]. It is worth to mentioning that the friction coefficient for the PEO SG 200 specimen is higher than that of the PEO SG 100 specimen despite its higher sol-gel thickness. We can explain this result to the higher topographic parameters and to the more heterogeneous thickness (Table 2) resulting in an uneven surface. In all cases, the friction coefficient is lower than that of the aluminum substrate (0.9 when sliding distance exceeds 200 m). Therefore, the sol-gel seems to be able to decrease the shear stresses in the coatings which improves wear resistance of PEO SG coatings.
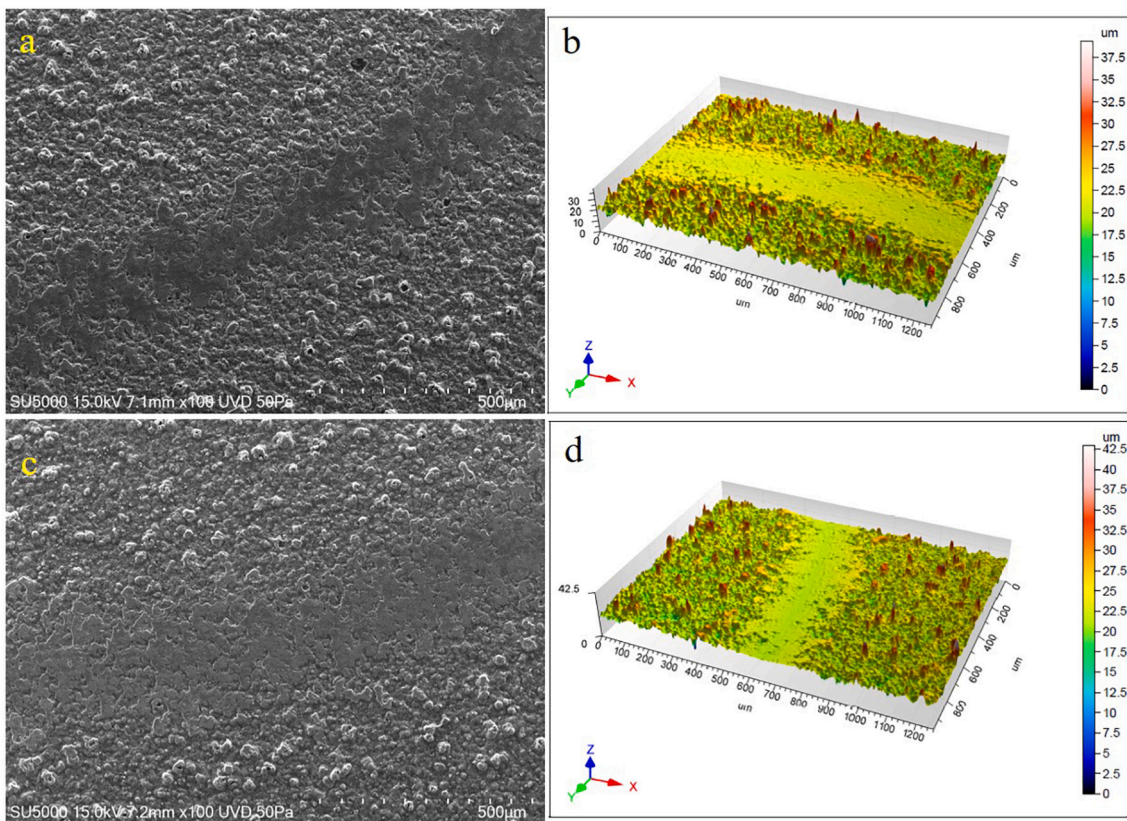
Fig. 6. Wear tracks obtained by SEM and wear 3D topographic surfaces obtained by confocal microscopy for PEO SG specimens. (a) and (b) PE0 SG 100. (c) and (d) PEO SG 200.
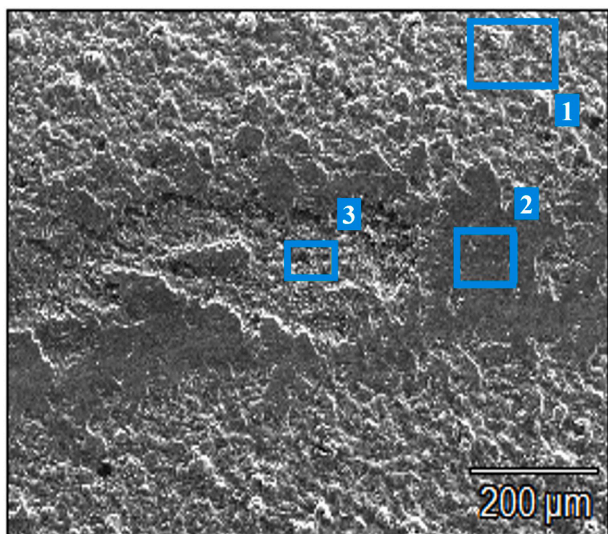

Fig. 7. SEM image of the wear track on the unsealed PEO sample and the respective EDX analysis zones.

Table 3
Chemical composition of the wear track by EDX analysis.

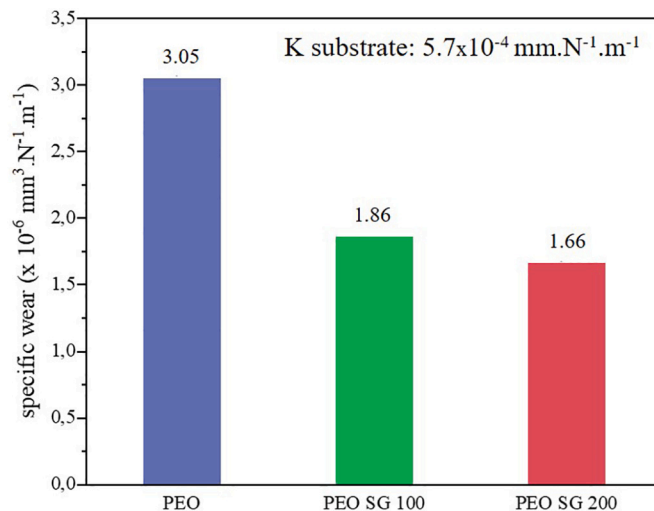| Analysis zone	Composition (% at.)							
	Al	O	Mg	Cu	Si	Ca	K	Mn
1	32.54	61.69	0.55	0.63	4.06	0.13	0.40	
2	32.39	65.05	0.54	0.30	1.60			0.12
3	37.22	60.61	0.48		1.50		0.19	

Fig. 8. Specific wear for PEO and PEO SG specimens.

Analysis of the wear tracks morphologies are presented in Fig. 5 for PEO coating and Fig. 6 for PEO coatings sealed with sol-gel. Wear tracks observed by SEM show the absence of parallel lines meaning that no abrasion mechanism occurs in the contact. However, an even flattening of the roughness was observed resulting from interfacial shearing without or probably with very few removal or pullout of material for PEO SG samples. The same kind of surface morphology of wear tracks was obtained by Javidi & Fadaee [59] for PEO coatings on AA2024. The superficial layer, also called third body, acts as accommodation mechanism for the relative displacement between the coating and the

counterbody. In the case of PEO coatings, again we observed flattening of the roughness (Fig. 5a, b) but also many delamination areas (Fig. 5c, d and e).

A magnification of the delamination zone is shown in Fig. 7, and the respective EDX analysis are shown in Table 3. It is obvious that the third body disbonding can be attributed to cracking of the PEO layer resulting in pullout of debris. The chemical analysis in the zone 1, outside of the wear track, is identical to the results obtained in the surface analysis. Moreover, the results have shown that the elemental distribution inside the delamination zones, on the flattened zone and outside of the wear tracks are close to alumina, meaning that alumina remains inside the delamination zone and so only the third body was pulled out and ejected from the contact. The latter element highlights the good adhesion of the PEO coating on the substrate.

The specific wear rates for the substrate and the coated materials are summarized in Fig. 8. In the case of PEO samples, the calculation of the wear volume takes into account the two different areas, i.e. flattening zones and delamination zones. Specific wear rates for coated specimens varying between 1.66×10^{-6} and 3.05×10^{-6} mm^3.N^{-1}.m^{-1} are very low compared to the substrate (5.7×10^{-4} mm^3.N^{-1}.m^{-1}). Also, we can notice a benefit of sol-gel filling as the specific wear rate decreased by about 40% for PEO SG coatings compared to the PEO coating. J. A. Curran and T. H. Clyne have studied the influence of the porosity and of the microcracks on the stiffness and the hardness of PEO alumina coatings [46,60]. They have shown that the porosities and the microcracks inside the alumina are the cause of a reduction in stiffness by an order of magnitude compared to a fully dense alumina. The sol-gel layer fills the porosities and microcracks and likely acts as a cement that strengthens the coating. Therefore, these data demonstrate that the sol-gel filling improves the mechanical resistance of the PEO coatings. We can also attribute the improved wear resistance for PEO SG coatings to the decrease of the shear stresses in the coating due to the pores filling.

The corrosion behavior of the PEO with and without sol-gel coatings is shown in Fig. 9 after 1 h of immersion in 0.1 M Na$_2$SO$_4$. The corrosion behavior of the bare substrate is also shown for comparison reasons.

The difference in the size of the semi-circle diameter on the Nyquist plot denotes the higher corrosion resistance of the PEO coating sealed with sol-gel compared to the unsealed PEO coating and the bare AA2024 substrate (Fig. 9a). On the Bode plot, it is possible to see significant differences in the modulus and phase diagrams among the samples

(Fig. 9b and c). At low frequencies (10^{-1} Hz), the PEO sample presents an increase of the impedance value of just one order of magnitude compared to the bare AA2024 substrate: 10^6 Ω.cm^2 in comparison to 10^5 Ω.cm^2. The samples sealed with sol-gel presented a significantly higher impedance value: around 10^8 Ω.cm^2 at this frequency. On the phase diagram, the bare AA2024 presents just a one-time constant associated with the passive layer on the aluminum surface, around 10 Hz. The PEO coated sample presents two-time constants, one at 10 Hz and another at higher frequencies, associated with the thicker PEO oxide coating. The samples sealed with sol-gel presented a one-time constant at higher frequencies, denoting the sol-gel layer's barrier property which is more specifically related to the impregnation of the PEO layer porosity by the sol-gel solution before curing. It is well known that barrier coatings prevent aggressive species from reaching the underneath substrate and initiating the corrosion process [61].

The stability of the corrosion resistance of the coatings was assessed up to 28 days of immersion in 0.1 M Na$_2$SO$_4$ (Fig. 10). For the unsealed PEO coating, the time evolution of modulus and phase angle (Fig. 10a and b) shows a change in behavior during the 14 first days. After seven days of immersion, the impedance decreases significantly, followed by a decrease in the phase of the time constant around 10 Hz. After 14 days, the impedance at low frequency (10^{-1} Hz) becomes comparable to the one of the bare AA2024 substrate. The time constant at higher frequencies is depressed but still observable. For the sol-gel coated samples (Fig. 10c–f), the same trend is observed. A decrease in the impedance and overall values of phase are observed only on the first seven days of immersion. After 28 days of immersion, the sol-gel layer's impedance values applied at 100 mm/min (Fig. 10c and d) are slightly superior to the ones from the sol-gel layer applied at 200 mm/min (Fig. 10e and f). The experimental data were fitted to electrical equivalent circuits (EEC), as shown in Fig. 9d and e, where R_{Sol} is the solution resistance, CPE_{Out} is the constant phase element from the outmost coating layer, R_{Out} is the resistance of the outmost coating layer, CPE_{Int} is the constant phase element from the internal coating layer, R_{Int} is the resistance of the internal coating layer, CPE_{Inner} is the constant phase element related to the electrical double-layer, and R_{Inner} is the charge transfer resistance. In the EEC fitting procedure, all the capacitances were replaced by constant phase elements (CPE) to consider the non-ideality of the system. Eq. (2) is used for the impedance of a constant phase element [62].
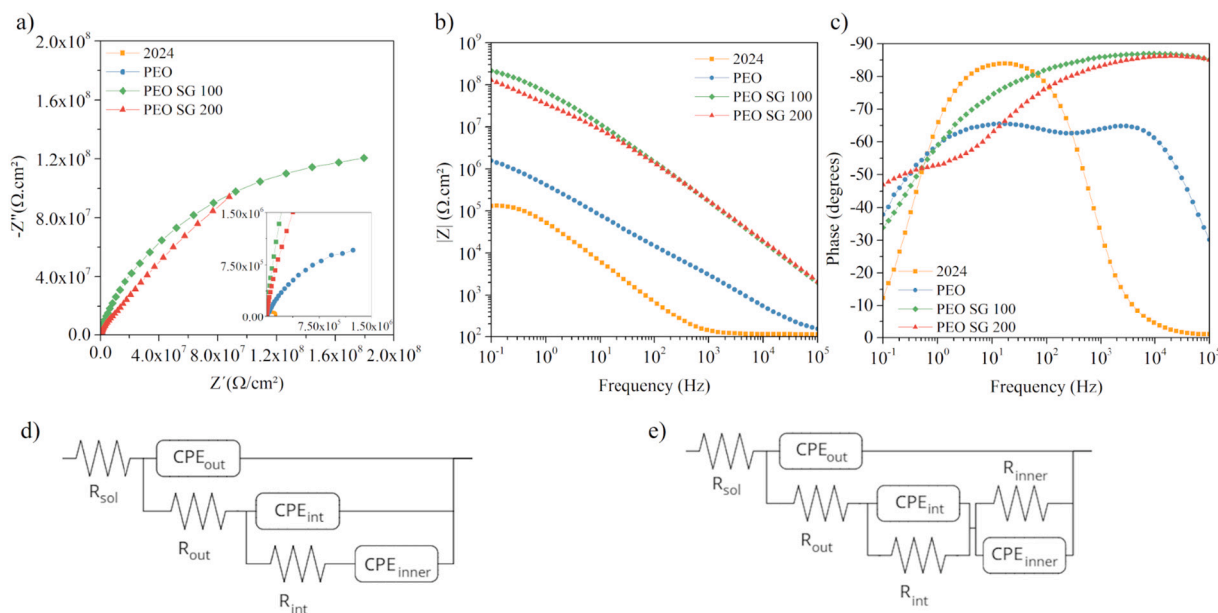

Fig. 9. Nyquist (a) and Bode (b, c) plots of the coatings after 1 h of immersion in 0.1 M Na$_2$SO$_4$. Equivalent electric circuits used for fitting the experimental EIS data (d, e).
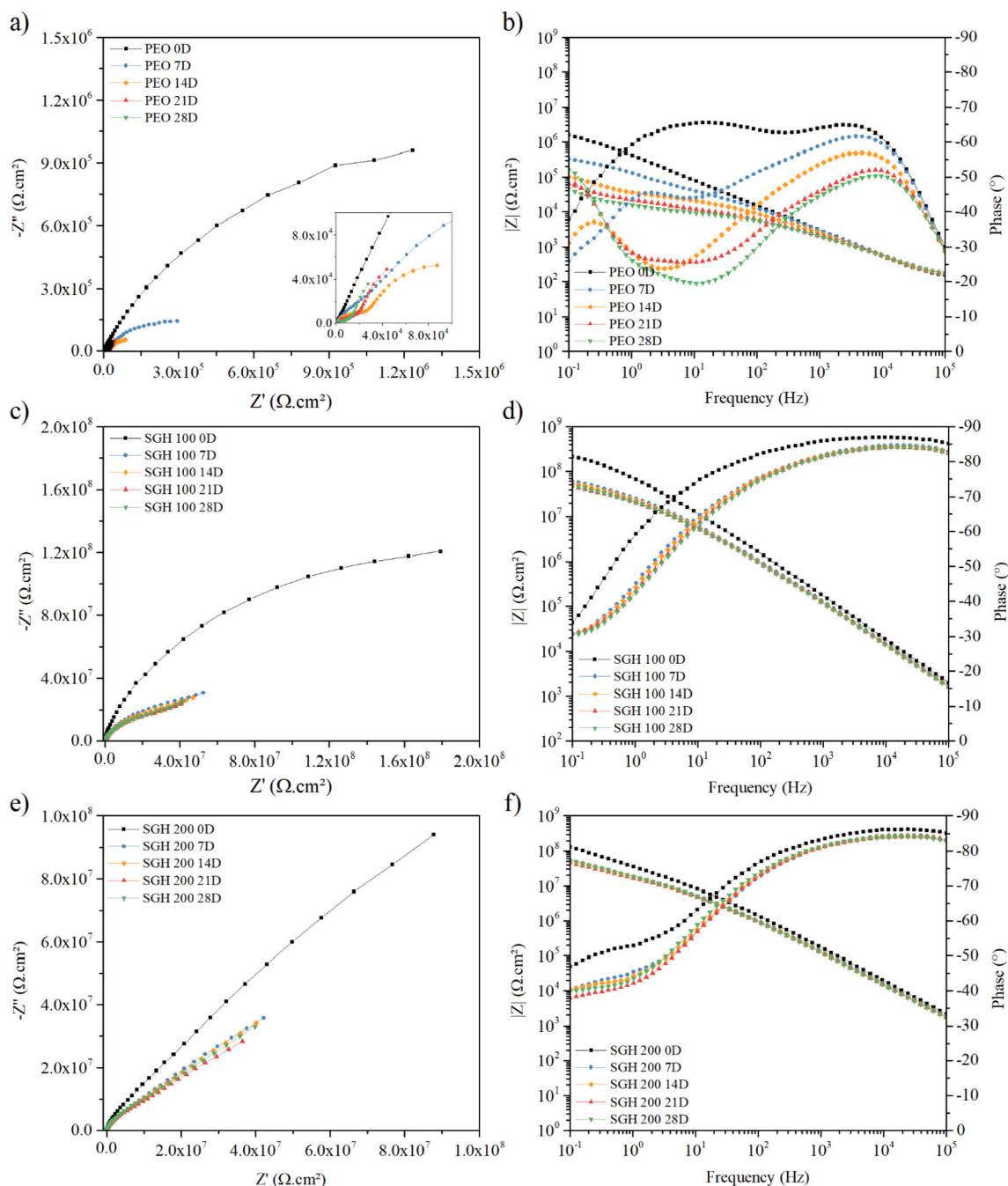
Fig. 10. EIS bode plots of the PEO (a, b), PEO sealed with sol-gel applied at 100 mm/min (c, d) and PEO sealed with sol-gel applied at 200 mm/min (e, f), until 28 days of immersion in 0.1 M Na$_2$SO$_4$.

$$Z_{CPE} = \frac{1}{Y_0(iw)^n} \qquad (2)$$

The parameter n is the frequency dispersion factor and takes values between 0 and 1. When n = 1, the CPE is a pure capacitance and corresponds to a pure resistance when n = 0 [62]. The EEC from Fig. 9d was used to fit the data from PEO samples at day 0. Since the corrosion medium has not yet completely penetrated the coating porous, the EEC resembles a circuit with two-time constants where CPE$_{Inner}$ is not yet considered. From 7 to 28 days of immersion, the data from the unsealed PEO sample was fitted using the EEC from Fig. 9e, in good agreement with the literature [63]. For extended immersion times the electrolyte can easily penetrate to the aluminum coating and easily reach the metallic interface, creating a short-circuit pathway, precluding the

determination of R$_{Out}$ and R$_{Int}$ [64] which become negligible. The experimental data from the samples sealed with sol-gel were fitted using the EEC from Fig. 9d. Similar to the unsealed PEO samples at day 0, the resistor and the constant phase element related to the inner parts of layer were not considered due to insufficient electrolyte penetration. Table 4 presents the EIS fitted parameters. The increased values of R$_{Out}$ and R$_{Int}$ on samples with sol-gel, along with the smaller values of CPE, are in good agreement with the trends observed in the EIS plots. Moreover, the evolution of the values of R$_{Out}$ and R$_{Int}$ during the immersion time revels the protective nature of the sol-gel layers. These values are several orders of magnitude higher than for the PEO coatings confirming that the sol-gel layer is able to fill in the pores of the PEO coating and to increase the barrier properties of the duplex coating layer. Due to the specific and

Table 4
EIS parameters fitted from the equivalent circuits.

Sample		Rsol	CPE$_{Out}$	nOut	ROut	CPE$_{Int}$	nInt	RInt	CPEInner	nInner	RInner
		Ohm.cm^2	F.cm^{-2}.s$^{(n-1)}$		Ohm.cm^2	F.cm^{-2}.s$^{(n-1)}$		Ohm.cm^2	F.cm^{-2}.s$^{(n-1)}$		Ohm.cm^2
PEO	D0	109.50	2.18E−7	0.82	1.1E4	3.63E−7	0.68	2.93E6	–	–	–
	D7	119.20	2.07E−7	0.82	7582	7.31E−7	0.71	17,334	2.02E−6	0.65	4.72E5
	D14	118.5	2.71E−7	0.80	3587	2.93E−6	0.50	30,558	1.36E−5	0.89	1.18E5
	D21	115.3	1.84E−7	0.81	–	1.37E−5	0.29	36,940	3.07E−5	0.95	1.68E5
	D28	104.0	6.51E−7	0.72	–	5.37E−5	0.14	–	4.72E−5	0.93	1.42E5
PEO SG 100	D0	82.29	1.16E−9	0.97	2.92E6	2.95E−9	0.53	4.46E8	–	–	–
	D7	78.70	1.79E−9	0.95	8.28E5	7.87E−9	0.55	6.84E7	3.76E−8	0.51	–
	D14	71.65	1.99E−9	0.94	9.19E5	8.56E−9	0.54	5.79E7	3.88E−8	0.50	–
	D21	76.12	2.00E−9	0.94	6.65E5	1.09E−8	0.51	6.17E7	5.58E−8	0.69	–
	D28	74.83	2.09E−9	0.94	8.96E5	9.52E−9	0.53	5.06E7	4.16E−8	0.52	–
PEO SG 200	D0	85.72	1,26E−9	0.96	2.56E6	9.21E−9	0.49	–	–	–	–
	D7	76.15	1.67E−9	0.95	7.47E5	3.71E−9	0.65	4.63E6	1.94E−8	0.42	–
	D14	74.86	1.79E−9	0.95	5.05E5	9.92E−9	0.52	1.56E7	1.53E−8	0.43	–
	D21	56.19	1.88E−9	0.95	5.72E5	8.82E−9	0.54	1.95E6	1.33E−9	0.41	–
	D28	75.72	1.83E−9	0.95	4.04E5	1.21E−8	0.50	3.31E7	1.52E−8	0.48	–

gradual porosity of the PEO layer, different time constants need to be used to describe the equivalent electrical circuit of the layer. It is worth to mentioning that in the case of the PEO-SG layers, the values of the R$_{inner}$ are no more useful to describe the electrical behavior. The n values of the internal and inner layer CPE are close to 0.5. Such value is often associated with a diffusion-controlled process but based on the literature investigating the EIS behavior of sealed classical anodic porous layer, this low value can also be related to the complex nature of the layer showing a porous structure that could be represented by a transmission line element [65].

4. Conclusions

The sealing ability of two sol-gel layers on AA2024 PEO coatings were investigated. The sol-gel ability to fill PEO pores and micro-cracks is independent of the withdrawal rate used on the application, although a more homogeneous coverage is observed on layers applied with lower withdrawal rates. EIS results show the uncoated PEO coating fails to ensure a long-term barrier property, while the sol-gel sealed PEO layers sustained the protective behavior upon 28 days of immersion and increased the resistance of the system by several orders of magnitude in comparison to unsealed PEO coatings. The sol-gel layer filled the PEO porosities and microcracks and acted as a cement, decreasing the shear stresses of the coating and improving its tribological properties. A decrease of 40% in the wear rate was observed in PEO coatings sealed with sol-gel compared to unsealed PEO. Those results show the viability of using sol-gel layers to seal PEO coatings obtained in AA2024, increasing its corrosion resistance along with improving its tribological properties.

CRediT authorship contribution statement

Luciane Sopchenski: Conceptualization, Methodology, Investigation, Formal analysis, Data curation, Writing. Julien Robert: Investigation, Data curation. Matthieu Touzin: Investigation, Data curation. Arnaud Tricoteaux: Methodology, Investigation, Supervision, Formal analysis, Writing. Marie-Georges Olivier: Conceptualization, Methodology, Formal analysis, Writing, Supervision.

Declaration of competing interest

The authors declare that they have no known competing financial interests or personal relationships that could have appeared to influence the work reported in this paper.

Appendix A. Supplementary data

Supplementary data to this article can be found online at https://doi.org/10.1016/j.surfcoat.2021.127195.

References

[1] N. Murer, R. Oltra, B. Vuillemin, O. Néel, Numerical modelling of the galvanic coupling in aluminium alloys: a discussion on the application of local probe techniques, Corros. Sci. (2010), https://doi.org/10.1016/j.corsci.2009.08.051.

[2] X. Zhang, X. Zhou, T. Hashimoto, B. Liu, Localized corrosion in AA2024-T351 aluminium alloy: transition from intergranular corrosion to crystallographic pitting, Mater. Charact. (2017), https://doi.org/10.1016/j.matchar.2017.06.022.

[3] K.A. Yasakau, J. Tedim, M.L. Zheludkevich, M.G.S. Ferreira, Smart self-healing coatings for corrosion protection of aluminium alloys, in: Handb. Smart Coatings Mater. Prot, Elsevier, 2014, pp. 224–274, https://doi.org/10.1533/9780857096883.2.224.

[4] A.L. Yerokhin, X. Nie, A. Leyland, A. Matthews, S.J. Dowey, Plasma electrolysis for surface engineering, Surf. Coat. Technol. 122 (1999) 73–93, https://doi.org/10.1016/S0257-8972(99)00441-7.

[5] D.V. Mashtalyar, K.V. Nadaraia, A.S. Gnedenkov, I.M. Imshinetskiy, M.A. Piatkova, A.I. Pleshkova, E.A. Belov, V.S. Filonina, S.N. Suchkov, S.L. Sinebryukhov, S.V. Gnedenkov, Bioactive coatings formed on titanium by plasma electrolytic oxidation: composition and properties, Materials (Basel) 13 (2020) 4121, https://doi.org/10.3390/ma13184121.

[6] S. Stojadinović, R. Vasilić, M. Perić, Investigation of plasma electrolytic oxidation on valve metals by means of molecular spectroscopy – a review, RSC Adv. 4 (2014) 25759–25789, https://doi.org/10.1039/C4RA03873H.

[7] L. Wang, L. Chen, Z. Yan, W. Fu, Optical emission spectroscopy studies of discharge mechanism and plasma characteristics during plasma electrolytic oxidation of magnesium in different electrolytes, Surf. Coat. Technol. 205 (2010) 1651–1658, https://doi.org/10.1016/j.surfcoat.2010.10.022.

[8] L. Snizhko, A. Yerokhin, A. Pilkington, N. Gurevina, D. Misnyankin, A. Leyland, A. Matthews, Anodic processes in plasma electrolytic oxidation of aluminium in alkaline solutions, Electrochim. Acta 49 (2004) 2085–2095, https://doi.org/10.1016/j.electacta.2003.11.027.

[9] M. Mohedano, X. Lu, E. Matykina, C. Blawert, R. Arrabal, M.L. Zheludkevich, Plasma electrolytic oxidation (PEO) of metals and alloys, Encycl. Interfacial Chem. Surf. Sci. Electrochem. (2018) 423–438, https://doi.org/10.1016/B978-0-12-409547-2.13398-0.

[10] M.H. Zhu, Z.B. Cai, X.Z. Lin, P.D. Ren, J. Tan, Z.R. Zhou, Fretting wear behaviour of ceramic coating prepared by micro-arc oxidation on Al–Si alloy, Wear. 263 (2007) 472–480, https://doi.org/10.1016/j.wear.2007.01.050.

[11] X. Nie, E.I. Meletis, J.C. Jiang, A. Leyland, A.L. Yerokhin, A. Matthews, Abrasive wear/corrosion properties and TEM analysis of Al$_2$O$_3$ coatings fabricated using plasma electrolysis, Surf. Coat. Technol. (2002), https://doi.org/10.1016/S0257-8972(01)01453-0.

[12] M. Treviño, R.D. Mercado-Solis, R. Colás, A. Pérez, J. Talamantes, A. Velasco, Erosive wear of plasma electrolytic oxidation layers on aluminium alloy 6061, Wear (2013), https://doi.org/10.1016/j.wear.2012.12.011.

[13] Q.B. Li, C.C. Liu, W.B. Yang, J. Liang, Growth mechanism and adhesion of PEO coatings on 2024Al alloy, Surf. Eng. 33 (2017) 760–766, https://doi.org/10.1080/02670844.2016.1200860.

[14] K. Du, X. Guo, Q. Guo, F. Wang, Y. Tian, A monolayer PEO coating on 2024 Al alloy by transient self-feedback control mode, Mater. Lett. 91 (2013) 45–49, https://doi.org/10.1016/j.matlet.2012.09.055.

[15] V. Ntomprougkidis, J. Martin, A. Nominé, G. Henrion, Sequential run of the PEO process with various pulsed bipolar current waveforms, Surf. Coat. Technol. 374 (2019) 713–724, https://doi.org/10.1016/j.surfcoat.2019.06.057.

[16] M. Mohedano, M. Serdechnova, M. Starykevich, S. Karpushenkov, A.C. Bouali, M. G.S. Ferreira, M.L. Zheludkevich, Active protective PEO coatings on AA2024: role of voltage on in-situ LDH growth, Mater. Des. 120 (2017) 36–46, https://doi.org/10.1016/j.matdes.2017.01.097.

[17] W. Dai, C. Li, D. He, D. Jia, Y. Zhang, Z. Tan, Influence of duty cycle on fatigue life of AA2024 with thin coating fabricated by micro-arc oxidation, Surf. Coat. Technol. (2019), https://doi.org/10.1016/j.surfcoat.2018.12.118.

[18] A. Fattah-alhosseini, S.O. Gashti, M. Molaie, Effects of disodium phosphate concentration (Na$_2$HPO$_4$·2H$_2$O) on microstructure and corrosion resistance of plasma electrolytic oxidation (PEO) coatings on 2024 Al alloy, J. Mater. Eng. Perform. 27 (2018) 825–834, https://doi.org/10.1007/s11665-018-3124-1.

[19] P. Zhang, Y. Zuo, G. Nie, The pore structure and properties of microarc oxidation films on 2024 aluminum alloy prepared in electrolytes with oxide nanoparticles, J. Alloys Compd. 816 (2020) 152520, https://doi.org/10.1016/j.jallcom.2019.152520.

[20] V.M. Posuvailo, V.V. Kulyk, Z.A. Duriagina, I.V. Koval'chuck, M.M. Student, B. D. Vasyliv, The effect of electrolyte composition on the plasma electrolyte oxidation and phase composition of oxide ceramic coatings formed on 2024 aluminium alloy, Arch. Mater. Sci. Eng. 2 (2020) 49–55, https://doi.org/10.5604/01.3001.0014.5761.

[21] I. Shchedrina, A.G. Rakoch, G. Henrion, J. Martin, Non-destructive methods to control the properties of MAO coatings on the surface of 2024 aluminium alloy, Surf. Coat. Technol. 238 (2014) 27–44, https://doi.org/10.1016/j.surfcoat.2013.10.032.

[22] R. del Olmo, M. Mohedano, P. Visser, E. Matykina, R. Arrabal, Flash-PEO coatings loaded with corrosion inhibitors on AA2024, Surf. Coat. Technol. 402 (2020) 126317, https://doi.org/10.1016/j.surfcoat.2020.126317.

[23] X. Wu, W. Qin, Y. Guo, Z. Xie, Self-lubricative coating grown by micro-plasma oxidation on aluminum alloys in the solution of aluminate–graphite, Appl. Surf. Sci. 254 (2008) 6395–6399, https://doi.org/10.1016/j.apsusc.2008.04.001.

[24] B.L. Jiang, Y.M. Wang, Plasma electrolytic oxidation treatment of aluminium and titanium alloys, in: Surf. Eng. Light Alloy, Elsevier, 2010, pp. 110–154, https://doi.org/10.1533/9781845699451.2.110.

[25] M. Sieber, F. Simchen, R. Morgenstern, I. Scharf, T. Lampke, Plasma electrolytic oxidation of high-strength aluminium alloys—substrate effect on wear and corrosion performance, Metals (Basel) 8 (2018) 356, https://doi.org/10.3390/met8050356.

[26] S. Ignjatović, C. Blawert, M. Serdechnova, S. Karpushenkov, M. Damjanović, P. Karlova, D.C.F. Wieland, M. Starykevich, S. Stojanović, L. Damjanović-Vasilić, M.L. Zheludkevich, Formation of multi-functional TiO$_2$ surfaces on AA2024 alloy using plasma electrolytic oxidation, Appl. Surf. Sci. 544 (2021) 148875, https://doi.org/10.1016/j.apsusc.2020.148875.

[27] M. Javidi, H. Fadaee, Plasma electrolytic oxidation of 2024-T3 aluminum alloy and investigation on microstructure and wear behavior, Appl. Surf. Sci. (2013), https://doi.org/10.1016/j.apsusc.2013.09.049.

[28] W. Xue, J. Du, X. Wu, Y. Lai, Tribological behavior of microarc oxidation coatings on aluminum alloy, ISIJ Int. 46 (2006) 287–291, https://doi.org/10.2355/isijinternational.46.287.

[29] L. Wen, Y. Wang, Y. Zhou, J.H. Ouyang, L. Guo, D. Jia, Corrosion evaluation of microarc oxidation coatings formed on 2024 aluminium alloy, Corros. Sci. 52 (2010) 2687–2696, https://doi.org/10.1016/j.corsci.2010.04.022.

[30] D.V. Mashtalyar, K.V. Nadaraia, I.M. Imshinetskiy, E.A. Belov, V.S. Filonina, S. N. Suchkov, S.L. Sinebryukhov, S.V. Gnedenkov, Composite coatings formed on Ti by PEO and fluoropolymer treatment, Appl. Surf. Sci. 536 (2021) 147976, https://doi.org/10.1016/j.apsusc.2020.147976.

[31] J. Joo, D. Kim, H.-S. Moon, K. Kim, J. Lee, Durable anti-corrosive oil-impregnated porous surface of magnesium alloy by plasma electrolytic oxidation with hydrothermal treatment, Appl. Surf. Sci. 509 (2020) 145361, https://doi.org/10.1016/j.apsusc.2020.145361.

[32] L. Pezzato, R. Babbolin, P. Cerchier, M. Marigo, P. Dolcet, M. Dabalà, K. Brunelli, Sealing of PEO coated AZ91magnesium alloy using solutions containing neodymium, Corros. Sci. 173 (2020) 108741, https://doi.org/10.1016/j.corsci.2020.108741.

[33] B. Mingo, R. Arrabal, M. Mohedano, Y. Llamazares, E. Matykina, A. Yerokhin, A. Pardo, Influence of sealing post-treatments on the corrosion resistance of PEO coated AZ91 magnesium alloy, Appl. Surf. Sci. 433 (2018) 653–667, https://doi.org/10.1016/j.apsusc.2017.10.083.

[34] L. Pezzato, K. Brunelli, R. Babbolin, P. Dolcet, M. Dabalà, Sealing of PEO coated AZ91 magnesium alloy using La-based solutions, Int. J. Corros. 2017 (2017) 1–13, https://doi.org/10.1155/2017/5305218.

[35] T. Li, L. Li, J. Qi, F. Chen, Corrosion protection of Ti6Al4V by a composite coating with a plasma electrolytic oxidation layer and sol-gel layer filled with graphene oxide, Prog. Org. Coat. 144 (2020) 105632, https://doi.org/10.1016/j.porgcoat.2020.105632.

[36] M. Toorani, M. Aliofkhazraei, Review of electrochemical properties of hybrid coating systems on mg with plasma electrolytic oxidation process as pretreatment, Surf. Interfac. 14 (2019) 262–295, https://doi.org/10.1016/j.surfin.2019.01.004.

[37] S. Farshid, M. Kharaziha, Micro and nano-enabled approaches to improve the performance of plasma electrolytic oxidation coated magnesium alloys, J. Magnes. Alloy (2020), https://doi.org/10.1016/j.jma.2020.11.004.

[38] H. Duan, K. Du, C. Yan, F. Wang, Electrochemical corrosion behavior of composite coatings of sealed MAO film on magnesium alloy AZ91D, Electrochim. Acta (2006), https://doi.org/10.1016/j.electacta.2005.08.026.

[39] W. Shang, B. Chen, X. Shi, Y. Chen, X. Xiao, Electrochemical corrosion behavior of composite MAO/sol-gel coatings on magnesium alloy AZ91D using combined micro-arc oxidation and sol-gel technique, J. Alloys Compd. (2009), https://doi.org/10.1016/j.jallcom.2008.06.135.

[40] L. Pezzato, M. Rigon, A. Martucci, K. Brunelli, M. Dabalà, Plasma Electrolytic Oxidation (PEO) as pre-treatment for sol-gel coating on aluminum and magnesium alloys, Surf. Coat. Technol. 366 (2019) 114–123, https://doi.org/10.1016/j.surfcoat.2019.03.023.

[41] D. Zeng, Z. Liu, S. Bai, J. Wang, Influence of sealing treatment on the corrosion resistance of PEO coated Al-Zn-Mg-Cu alloy in various environments, Coatings. 9 (2019) 867, https://doi.org/10.3390/coatings9120867.

[42] A.C. Bouali, E.A. Straumal, M. Serdechnova, D.C.F. Wieland, M. Starykevich, C. Blawert, J.U. Hammel, S.A. Lermontov, M.G.S. Ferreira, M.L. Zheludkevich, Layered double hydroxide based active corrosion protective sealing of plasma electrolytic oxidation/sol-gel composite coating on AA2024, Appl. Surf. Sci. 494 (2019) 829–840, https://doi.org/10.1016/j.apsusc.2019.07.117.

[43] H. Costenaro, F.M. Queiroz, M. Terada, M.G. Olivier, I. Costa, H.G. De Melo, Corrosion protection of AA2524-T3 anodized in tartaric-sulfuric acid bath and protected with hybrid sol-gel coating, Key Eng. Mater. 710 (2016) 210–215, https://doi.org/10.4028/www.scientific.net/KEM.710.210.

[44] V. Dehnavi, D.W. Shoesmith, B.L. Luan, M. Yari, X.Y. Liu, S. Rohani, Corrosion properties of plasma electrolytic oxidation coatings on an aluminium alloy - the effect of the PEO process stage, Mater. Chem. Phys. 161 (2015) 49–58, https://doi.org/10.1016/j.matchemphys.2015.04.058.

[45] A. Fattah-Alhosseini, M. Vakili-Azghandi, M.K. Keshavarz, Influence of concentrations of KOH and Na$_2$SiO$_3$ electrolytes on the electrochemical behavior of ceramic coatings on 6061 Al alloy processed by plasma electrolytic oxidation, Acta Metall. Sin. (English Lett.) 29 (2016) 274–281, https://doi.org/10.1007/s40195-016-0384-3.

[46] J.A. Curran, T.W. Clyne, Thermo-physical properties of plasma electrolytic oxide coatings on aluminium, Surf. Coat. Technol. 199 (2005) 168–176, https://doi.org/10.1016/j.surfcoat.2004.09.037.

[47] V.S. Egorkin, S.V. Gnedenkov, S.L. Sinebryukhov, I.E. Vyaliy, A.S. Gnedenkov, R. G. Chizhikov, Increasing thickness and protective properties of PEO-coatings on aluminum alloy, Surf. Coat. Technol. 334 (2018) 29–42, https://doi.org/10.1016/j.surfcoat.2017.11.025.

[48] M. Serdechnova, S. Karpushenkov, L. Karpushenkava, M. Starykevich, M. Ferreira, T. Hack, M. Iuzviuk, I. Zobkalo, C. Blawert, M. Zheludkevich, The influence of PSA pre-anodization of AA2024 on PEO coating formation: composition, microstructure, corrosion, and wear behaviors, Materials (Basel) 11 (2018) 2428, https://doi.org/10.3390/ma11122428.

[49] F. Monfort, A. Berkani, E. Matykina, P. Skeldon, G.E. Thompson, H. Habazaki, K. Shimizu, Development of anodic coatings on aluminium under sparking conditions in silicate electrolyte, Corros. Sci. 49 (2007) 672–693, https://doi.org/10.1016/j.corsci.2006.05.046.

[50] M. Serdechnova, M. Mohedano, B. Kuznetsov, C.L. Mendis, M. Starykevich, S. Karpushenkov, J. Tedim, M.G..S. Ferreira, C. Blawert, M.L. Zheludkevich, PEO coatings with active protection based on in-situ formed LDH-nanocontainers, J. Electrochem. Soc. 164 (2017) C36–C45, https://doi.org/10.1149/2.0301702jes.

[51] R.O. Hussein, X. Nie, D.O. Northwood, A. Yerokhin, A. Matthews, Spectroscopic study of electrolytic plasma and discharging behaviour during the plasma electrolytic oxidation (PEO) process, J. Phys. D. Appl. Phys. 43 (2010) 105203, https://doi.org/10.1088/0022-3727/43/10/105203.

[52] R.H.U. Khan, A. Yerokhin, X. Li, H. Dong, A. Matthews, Surface characterisation of DC plasma electrolytic oxidation treated 6082 aluminium alloy: effect of current density and electrolyte concentration, Surf. Coat. Technol. 205 (2010) 1679–1688, https://doi.org/10.1016/j.surfcoat.2010.04.052.

[53] W. Xue, Z. Deng, Y. Lai, R. Chen, Analysis of phase distribution for ceramic coatings formed by microarc oxidation on aluminum alloy, J. Am. Ceram. Soc. 81 (1998) 1365–1368, https://doi.org/10.1111/j.1151-2916.1998.tb02493.x.

[54] Ľ. Smrčok, V. Langer, J. Křesťan, γ-Alumina: a single-crystal X-ray diffraction study, Acta Crystallogr. Sect. C Cryst. Struct. Commun. 62 (2006) i83–i84, https://doi.org/10.1107/S0108270106026850.

[55] N. Duboust, H. Ghadbeigi, C. Pinna, S. Ayvar-Soberanis, A. Collis, R. Scaife, K. Kerrigan, An optical method for measuring surface roughness of machined carbon fibre-reinforced plastic composites, J. Compos. Mater. (2017), https://doi.org/10.1177/0021998316644849.

[56] C.J. Brinker, A.J. Hurd, P.R. Schunk, G.C. Frye, C.S. Ashley, Review of sol-gel thin film formation, J. Non-Cryst. Solids 147–148 (1992) 424–436, https://doi.org/10.1016/S0022-3093(05)80653-2.

[57] X. Nie, A. Leyland, H.W. Song, A.L. Yerokhin, S.J. Dowey, A. Matthews, Thickness effects on the mechanical properties of micro-arc discharge oxide coatings on aluminium alloys, Surf. Coat. Technol. 116–119 (1999) 1055–1060, https://doi.org/10.1016/S0257-8972(99)00089-4.

[58] Q. Li, J. Liang, B. Liu, Z. Peng, Q. Wang, Effects of cathodic voltages on structure and wear resistance of plasma electrolytic oxidation coatings formed on aluminium

alloy, Appl. Surf. Sci. 297 (2014) 176–181, https://doi.org/10.1016/j.
apsusc.2014.01.120.

[59] M. Javidi, H. Fadaee, Plasma electrolytic oxidation of 2024-T3 aluminum alloy and investigation on microstructure and wear behavior, Appl. Surf. Sci. 286 (2013) 212–219, https://doi.org/10.1016/j.apsusc.2013.09.049.

[60] J.A. Curran, T.W. Clyne, Porosity in plasma electrolytic oxide coatings, Acta Mater. 54 (2006) 1985–1993, https://doi.org/10.1016/j.actamat.2005.12.029.

[61] A.M.A. Mohamed, A.M. Abdullah, N.A. Younan, Corrosion behavior of superhydrophobic surfaces: a review, Arab. J. Chem. 8 (2015) 749–765, https://doi.org/10.1016/j.arabjc.2014.03.006.

[62] G.E. Thompson, H. Habazaki, K. Shimizu, M. Sakairi, P. Skeldon, X. Zhou, G. C. Wood, Anodizing of aluminium alloys, Aircr. Eng. Aerosp. Technol. 71 (1999) 228–238, https://doi.org/10.1108/00022669910270709.

[63] G.A. Mengesha, J.P. Chu, B.-S. Lou, J.-W. Lee, Corrosion performance of plasma electrolytic oxidation grown oxide coating on pure aluminum: effect of borax concentration, J. Mater. Res. Technol. 9 (2020) 8766–8779, https://doi.org/10.1016/j.jmrt.2020.06.020.

[64] T.T. Thai, M.-E. Druart, Y. Paint, A.T. Trinh, M.-G. Olivier, Influence of the sol-gel mesoporosity on the corrosion protection given by an epoxy primer applied on aluminum alloy 2024–T3, Prog. Org. Coat. 121 (2018) 53–63, https://doi.org/10.1016/j.porgcoat.2018.04.013.

[65] G. Boisier, N. Pébère, C. Druez, M. Villatte, S. Suel, FESEM and EIS study of sealed AA2024 T3 anodized in sulfuric acid electrolytes: influence of tartaric acid, J. Electrochem. Soc. 155 (2008) C521, https://doi.org/10.1149/1.2969277.